IEEE Access
Multidisciplinary ⋮ Rapid Review ⋮ Open Access Journal

Received December 18, 2020, accepted January 16, 2021, date of publication January 26, 2021, date of current version February 12, 2021.

Digital Object Identifier 10.1109/ACCESS.2021.3054658

A Low-Cost Light-Weight Ultrawideband Wide-Angle Scanning Tightly Coupled Dipole Array Loaded With Multilayer Metallic Strips

ZHIGUO JIANG[1], (Student Member, IEEE), SHAOQIU XIAO[1,2], (Member, IEEE), AND BING-ZHONG WANG[1], (Senior Member, IEEE)

[1]School of Physics, University of Electronic Science and Technology of China, Chengdu 610054, China
[2]School of Electronics and Information Technology, Sun Yat-sen University, Guangzhou 510006, China

Corresponding author: Shaoqiu Xiao (xiaoshq8@mail.sysu.edu.cn)

This work was supported in part by the National Natural Science Foundation of China under Grant 61731005, in part by the Preresearch Foundation of National Defense under Grant 170441413086 and Grant 614240205070817, and in part by the Fundamental Research Funds for the Central Universities under Grant ZYGX2016Z008.

ABSTRACT This article presents a new ultrawideband wide-angle scanning tightly coupled dipole array loaded with multilayer metallic strips. The loaded multilayer metallic strips, which is composed of several narrow strips with different lengths, are used to equivalent the metal patch which has a specific shape. It can help achieve smoother impedance transform from the dipole to the free space. An equivalent circuit model (ECM) of the unit cell is proposed to help analyze and design the tightly coupled dipole array. Thanks to the loaded multilayer metallic strips, the array can be fed by a simple feeding structure, avoiding a matching network located below the ground plane. Also, all components of the proposed array are printed on a single dielectric substrate, resulting in a low-cost and light-weight array. The proposed tightly coupled dipole array can achieve 6.2:1 bandwidth with voltage stand wave ratio (VSWR) < 3 while scanning to $\pm 60°$ in all planes. The total profile of the array is 0.13 wavelength at 1.4 GHz. Finally, an 8×8 prototype is fabricated and measured. The measured results prove the feasibility of the design.

INDEX TERMS Ultrawideband array, wide-angle scanning array, tightly coupled dipole array.

I. INTRODUCTION

Ultrawideband wide-scan array can cover wide range in ultra-wide bandwidth, making it have important implications for the high-resolution imaging system [1] and multifunctional communication system [2]. As an implementation method, stacked patch antenna is used as the array element. The array can achieve over 2:1 bandwidth with $\pm 55°$ scanning [3]. Another popular wideband array is Vivaldi array. It can achieve about 10:1 bandwidth with $\pm 60°$ scanning. However, the traditional Vivaldi array suffer from subpar cross-polarization level when the array scanning in D-plane. Sliced notch Vivaldi array successfully improves the cross-polarization performance, while other electrically performance remains unchanged [4], [5]. Despite excellent performance, the array has a high profile, about $3\lambda_{high}$, where λ_{high} is the highest operating frequency of the array.

The associate editor coordinating the review of this manuscript and approving it for publication was Kuang Zhang.

Capacitively-coupled dipole array, also known as tightly coupled dipole array, which successfully achieves wheeler's current sheet [6], can achieve up to 9:1 bandwidth with a very low profile [7]. However, the original tightly coupled dipole array needs an external 180° hybrids or balun to avoid common-mode resonance, resulting in a high-cost feeding structure. To avoid external balun, several effective methods have been proposed. One effective method is using Marchand balun to excite the dipole [8]. Meanwhile, to reduce the dipole's input impedance, two dipoles are placed in a square unit cell and then fed by a power divider. With the dielectric loading, the array can achieve $\pm 45°$ scanning in 7.35:1 bandwidth. Afterwards, to avoid using power divider, a modified stripline-based Marchand balun with a stepped stripline impedance transform structure located below the ground plane is designed to achieve a wide-range impedance transform [9]. With the FSS structure loading, the array can achieve 6.1:1 bandwidth with $\pm 75°$ scanning in E-plane and $\pm 60°$ scanning in H-plane. Besides,

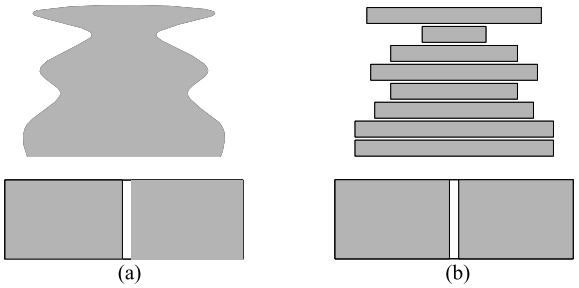

FIGURE 1. (a) The dipole loaded with the metal patch which has a specific shape. (b) The dipole with equivalent multilayer metallic strips loading.

other baluns, such as the balun based on Klopfenstein tapered microstrip lines [10] and coplanar strip line (CPS) to coplanar waveguide (CPW) balun [11], are designed to excite the tightly coupled dipole array, but they still need an impedance transform structure located below the ground plane. Although the stepped stripline can be horizontally placed on the ground plane, it increases the difficulty of the assembly [12]. Another effective method to avoid the external balun is using shorting vias or capacitively-loaded vias to remove the common-mode resonance out of the operating band [13], [14]. Although the array can be directly fed by coaxial, it's not suitable for low-frequency application due to the thick dielectric substrate.

In this article, a new tightly coupled dipole array loaded with a metal patch of specific shape is proposed. To facilitate the optimization of the shape of the loaded metal patch, the patch is divided into several narrow metallic strips in the design, as shown in Fig. 1. An equivalent circuit model (ECM) for the structure is proposed to help analyze and design the array. In the circuit model, the loaded metallic strips are modeled by the LC series circuits. They can provide a smoother impedance transform from the dipole to the free space, thus simplifying the feeding structure of the array. After careful design, the array can achieve 6.2:1 bandwidth while scanning to $\pm 60^\circ$ in all planes. Meanwhile, compared with the state-of-the-art wideband array, the proposed array has two advantages: 1) all the components are printed on a single dielectric substrate, resulting in a low-cost and light-weight array; and 2) all the components are placed above the ground plane, avoiding an impedance transform structure located below the ground plane.

This article is organized as follows. The basic element is analyzed in Section II. The designed element with feeding structure and its simulated results in infinite array is given in Section III. The simulated and measured results of the 8 $\times$ 8 prototype array is given in Section IV. Finally, it is the conclusion in Section V.

II. THE ANALYSIS OF THE BASIC ELEMENT

In the first step, to establish the equivalent circuit model, we consider the dipole loaded with horizontal metallic strips, as shown in Fig. 2(a). The metallic strips are loaded above a capacitively-coupled dipole. The equivalent circuit model of the proposed structure is shown in Fig. 2(b). In the equivalent

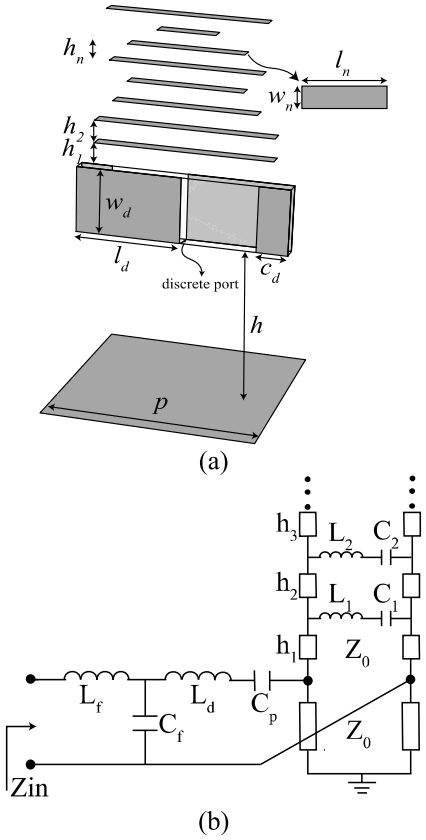

FIGURE 2. (a) The capacitively-coupled dipole loaded with multilayer metallic strips. (b) The equivalent circuit model.

model, the dipole and the coupling between the dipoles are equivalent to a LC series circuit, as proposed in [15]. On this basis, to make the equivalent circuit model more accurate, the capacitance introduced by the feeding gap and the inductance at the feeding position, which are represented by C_f and L_f, are added in the equivalent circuit model. Furthermore, the loaded metallic strip is modelled by a LC series circuit. The equivalent inductor and capacitor of the metallic strip can be calculated by the method developed by Marcuvitz [16]. The equations are given by,

$$\begin{cases} \dfrac{X_L}{Z_0} = \dfrac{1}{p} F(p, w_L, \lambda, \theta) \\ \dfrac{B_C}{Y_0} = 4\dfrac{w_c}{p} F(p, p-l, \lambda, \theta) \end{cases} \tag{1}$$

where

$$F(p, w, \lambda, \theta) = \frac{p}{\lambda}[\mathrm{In}(\csc\frac{\pi w}{2p}) + G(p, w, \lambda)] \tag{2}$$

$$G(p, w, \lambda, \theta) = \frac{1}{2} \times \frac{(1-\beta^2)^2[(1-\frac{\beta^2}{4})(A_+ + A_-) + 4\beta^2 A_+ A_-]}{(1-\frac{\beta^2}{4}) + \beta^2(1+\frac{\beta^2}{2}-\frac{\beta^4}{8})(A_+ + A_- + 2\beta^6 A_+ A_-)} \tag{3}$$

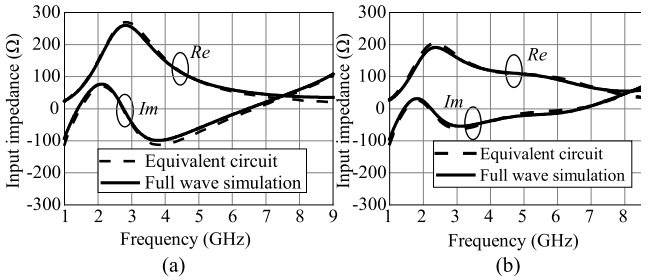

FIGURE 3. (a) The input impedance of the tightly coupled dipole without metallic strips loading. (b) The input impedance of the tightly coupled dipole with metallic strips loading.

with

$$\begin{cases} A_{\pm} = 1/\sqrt{1 \pm 2p \sin\theta/\lambda} - (p\cos\theta/\lambda)^2 - 1 \\ \beta = \sin(\pi w/2p) \end{cases} \tag{4}$$

where p, l, w, and θ represent the size of the unit cell, length of the metallic strip, width of the metallic strip, and the incident angle of the electromagnetic wave, respectively. $Z_0 = 1/Y_0$ is the characteristic impedance of the free space.

The proposed unit cell with fixed structural parameters is calculated to show the effect of the loaded metallic strips. The unit cell is a 15 mm × 15 mm square. The dipole is printed on a dielectric substrate with relative permittivity and thickness 2.2 and 1 mm. The height of the dipole above the ground plane is $h = 12.5$ mm. Other dipole's dimensions are given as follows, $c_d = 2.2$ mm, $l_d = 7.4$ mm, and $w_d = 5$ mm. Besides, the distance between the first metallic strip and the dipole is $h_1 = 2$ mm, and the distances between other metallic strips are all 1.2 mm. The lengths of the metallic strips are $l = [12.5, 12.5, 10, 8, 10.5, 8, 4, 11]$ mm. The widths of the metallic strips are fixed at 1 mm. In the equivalent circuit model, the value of the circuit components, which are corresponding to the dipole's dimensions, are selected to match with the input impedance calculated by full wave simulation, as shown in Fig. 3(a). The dipole's circuit parameters are given as follows, $L_f = 2.7$ nH, $C_f = 0.16$ pF, $L_p = 1.7$ nH, and $C_p = 0.6$ pF. Meanwhile, the distance between the dipole and the ground plane is 14.5 mm instead of 12.5 mm in the circuit model due to the vertical arrangement of the dipole. Also, the distance between the dipole and the first metallic strip is 3 mm instead of 2 mm in the circuit model. The circuit parameters of the metallic strips are calculated by equation (1). Meanwhile, to improve the accurate of the equivalent circuit model, an effective width 2.2 mm is used to replace actual width of the metal strip. Fig. 3(b) shows the input impedance of the dipole loaded with multilayer metallic strips calculated by full wave simulation and equivalent circuit, respectively. We found that the results calculated by equivalent circuit are agree well with the full wave simulation, proving the validity of the equivalent circuit model. More importantly, because the loaded metallic strips can provide a smooth impedance transform from the dipole to the free space, the dipole loaded with multilayer metallic strips has a lower and smoother input impedance, making the dipole can match with the coaxial

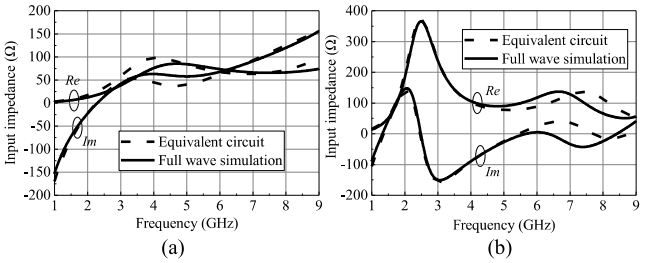

FIGURE 4. The input impedance of the tightly coupled dipole with metallic strips loading for E-/H-plane 60° scans calculated by equivalent circuit and full wave simulation. (a) E-plane. (b) H-plane.

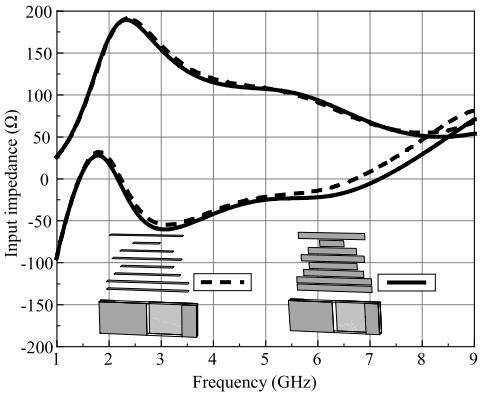

FIGURE 5. The input impedance of the tightly coupled dipole loaded with horizontal and vertical metallic strips.

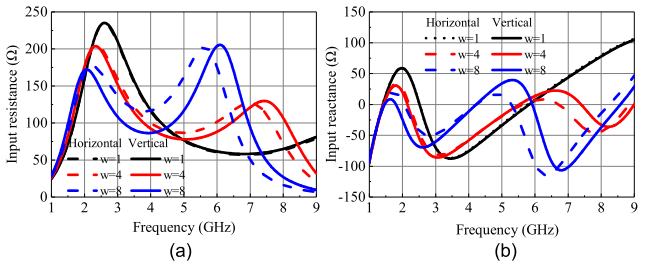

FIGURE 6. Impedance variation of the tightly coupled dipoles loaded with various width horizontal and vertical metallic strips. (a) Input resistance. (b) Input reactance.

more easily compared with the dipole without metallic strip loading. Besides, the input impedance of the dipole loaded with metallic strips for E- and H-planes 60° scans calculated by equivalent circuit model and full wave simulation are shown in Fig. 4. The impedance calculated by equivalent circuit agrees well with that obtained by full wave simulation, indicating that the proposed equivalent circuit model can also be used to analyze the scanning performance of the array.

In the second step, horizontal metallic strips are replaced by vertical metallic strips to achieve the structure with a single layer dielectric substrate. Because the vertical metallic strip can form the similar current distribution with the horizontal one with the dipole's excitation, the input impedances of the dipole loaded with two types of the metallic strips agree well with each other, as shown in Fig. 5. That means we can use the proposed equivalent circuit model for horizontal metallic strips loading to analyze the actual design. Fig. 6 shows the

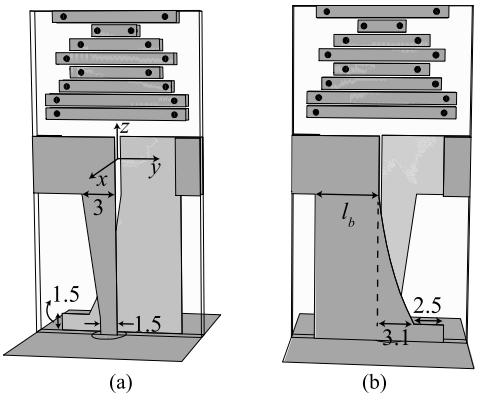

FIGURE 7. Proposed tightly coupled dipole array loaded with multilayer metallic strips. (a) Top view. (b) Bottom view.

input impedance of the dipole loaded with two types of metallic strip with different widths. It can be found that as the width increases, the difference between two types of metallic strip increases. In other words, not all horizontal metallic strip with arbitrary width can be replaced by a vertical one. To ensure the accuracy of the equivalent circuit analysis, the width of the loaded metallic strip is fixed at 1 mm in this design.

III. ANTENNA DESIGNS AND NUMERICAL SIMULATION

A. TIGHTLY COUPLED DIPOLE WITH FEEDING STRUCTURE

Fig. 7 shows the proposed tightly coupled dipole with the feeding structure. The whole structure is printed on the two sides of a single layer dielectric substrate, whose dielectric constant and thickness are 2.2 and 1 mm, respectively. The dimensions of the dipole and the loaded metallic strips are same with that analyzed in section II. A simple feeding structure, which uses a tapered line to achieve impedance transform from the dipole to coaxial, is designed to feed the dipole. The common-mode resonance caused by the unbalanced feeding structure can be removed out of the operating band by adding shorting vias between the neighboring elements [17]. In this design, the technology of mitigating common-mode resonance is integrated with the feeding structure, and the resonant frequency can be changed by adjusting l_b. As shown in Fig. 8, as l_b increases, the resonance frequency moves to higher frequency. Meanwhile, to improve the scanning performance in H-plane, two-sided metallic strips with shorting pins are used to replace one-sided metallic strips in the final design.

To ensure the profile of the array as low as possible, the width of the strips and the distance between the strips are fixed at 1 mm and 0.2 mm, respectively. First, the dipole with two-layer metallic strips loading is considered in the design. The lengths of the loaded strips are adjusted in the circuit model to obtain a smooth input impedance for both E- and H-planes scanning. Then the dipole with the feeding structure is calculated by the full wave simulation software. If the array cannot achieve good matching performance for both E- and H-planes scanning, we increase the layer of the strips. To further show the influence of the number of the

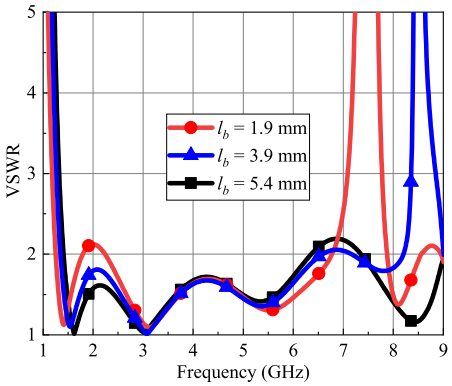

FIGURE 8. The VSWR for broadside radiation with different values of l_b.

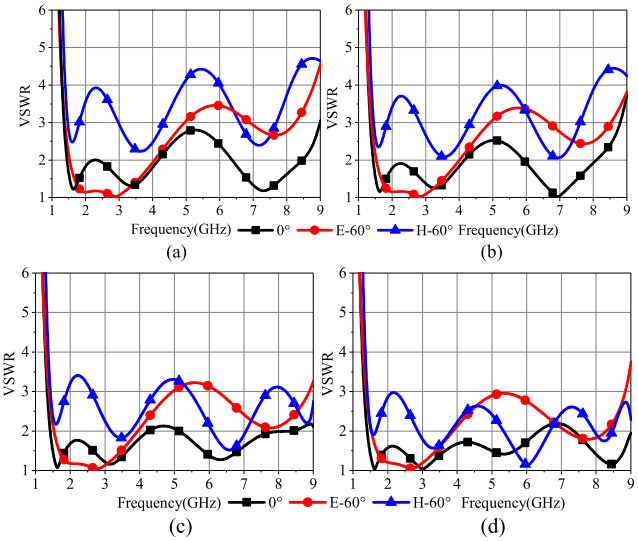

FIGURE 9. The VSWR of the array with different layers metallic strips loading. (a) Two layers. (b) Four layers. (c) Six layers. (d) Eight layers.

loaded strips on the matching performance of the array, the VSWRs with different layers metallic strips loading for 0°, E/H-plane 60° scans are shown in Fig. 9. It can be found that as the layers increases, the matching performance of the array becomes better in operating band. Meanwhile, when the metallic strips are increased to eight layers, the VSWR of the array is lower than 3 for both E- and H-planes scanning, which is acceptable for ultrawideband wide-angle scanning array. Besides, it should be noted that, when the impedance of the dipole matches with the feeding structure, the minimum VSWR will be obtained.

After careful design, the proposed element achieved a good matching performance for E- and H-planes scanning from 1.4 to 8.7 GHz. The size of the unit cell is $0.44\lambda_{high} \times 0.44\lambda_{high}$ and the total profile of the unit cell is $0.13\lambda_{low}$, where λ_{high} and λ_{low} are the highest and lowest operating frequency of the unit cell, respectively.

B. SIMULATED RESULTS OF THE INFINITE ARRAY

The unit cell with feeding structure is simulated in infinite array environment. It is well-known that the performance of

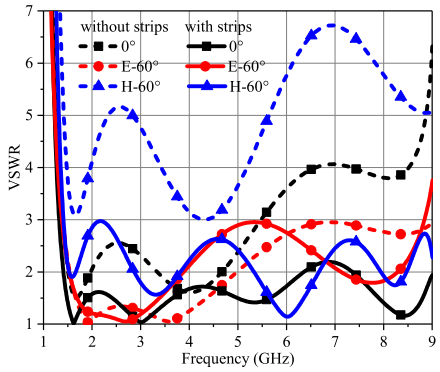

FIGURE 10. Comparison of the VSWR of the unit cell for broadside, E-/H-plane 60° scans with and without metallic strips loading.

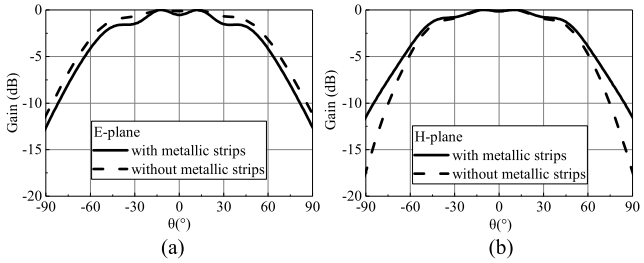

FIGURE 11. The active element pattern of the center element at 5 GHz with and without metallic strips loading. (a) E-plane. (b) H-plane.

the infinite array can be achieved with a finite array which has a large array size. Fig. 10 shows the simulated VSWR of the array with and without metallic strips loading for broadside, E-/H-plane 60° scans, respectively. It can be found that the array with metallic strips loading can scan up to 60° in all planes with VSWR < 3 from 1.4 to 8.7 GHz (6.2:1). Furthermore, the results indicate that the loaded metallic strips can improve the array matching performance obviously.

Generally, the active element pattern of a large array with element spacing less than half of the wavelength can be estimated by $G(\theta) = (4\pi A/\lambda^2)\cos\theta\,(1-|\Gamma(\theta)|^2)$, where A is the size of the unit cell, λ is the wavelength of operating frequency, and $\Gamma(\theta)$ is the active reflection coefficient for scan angle θ [18]. That means the active element pattern of a large array is decided by the active reflection coefficient. To further investigate the effect of the loaded strips on the active element pattern, $17\times\infty$ and $\infty\times 17$ arrays are calculated by full wave simulation, respectively. Fig. 11 shows the E- and H-planes active element pattern of the center element with and without strips loading at 5 GHz. For the E-plane pattern, the loaded metallic strips have almost no influence. For the H-plane pattern, the beam width of the pattern with metallic strips loading is wider than that without metallic strips loading, indicating that the loaded metallic strips have positive influence on the H-plane scanning. Furthermore, the comparison of the active VSWR shown in Fig. 10 indicates that the gain of the H-plane active element pattern with metallic strips loading is higher than that without metallic strips loading in operating band.

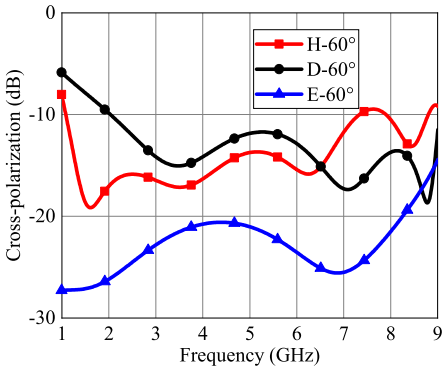

FIGURE 12. Normalized cross-polarization for scanning to 60° in E-, H-, and D-planes. The cross-polarization is defined by Lugwig's third definition.

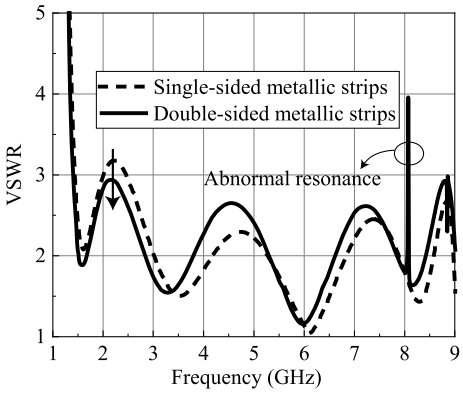

FIGURE 13. The contrast of the VSWR for scanning to 60° in H-plane with single-sided and double-sided metallic strips loading.

Fig. 12 shows the cross-polarization ratios, which is defined by Ludwig's third definition [19], for scanning to 60° in E-, H-, and D-planes. The curves show that the array can provide an average −20 dB, −15 dB, and −10 dB cross-polarization ratio for scanning to 60° in E-, H- and D-planes, respectively. Besides, the maximum cross-polarization ratios for scanning to 60° in E-, H-, and D-planes are -17 dB, -9.5 dB, and -7.5 dB, respectively.

C. ANALYSIS OF THE DOUBLE-SIDED METALLIC STRIP

In the final design, the loaded metallic strips are replaced by the double-sided metallic strips with shorting pins to decrease the maximum value of the VSWR for H-plane scanning. Fig. 13 shows the VSWR for scanning at 60° in H-plane with single-sided metallic strips and double-sided metallic strips loading. Note that the length and width of the strips are the same in both cases. We found that the double-sided metallic strips can help decrease the maximum value of the VSWR for scanning to 60° in H-plane. However, an abnormal resonance will appear at about 8 GHz in double-sided case. To explain the abnormal resonance, an equivalent circuit of the double-sided metallic strip for TE mode 60° incidence is given in Fig. 14(a). Different from the equivalent circuit for normal incidence, a transmission line, whose length is approximately equal to the thickness

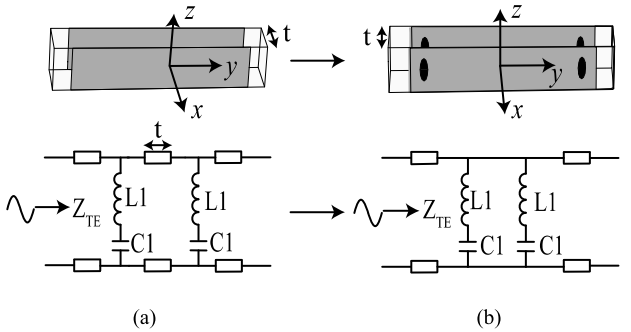

FIGURE 14. (a) The double-sided metallic strips and its equivalent circuit model for TE mode incidence in xoz-plane. (b) The double-sided metallic strips with shorting pins and its equivalent circuit model for TE mode incidence in xoz-plane.

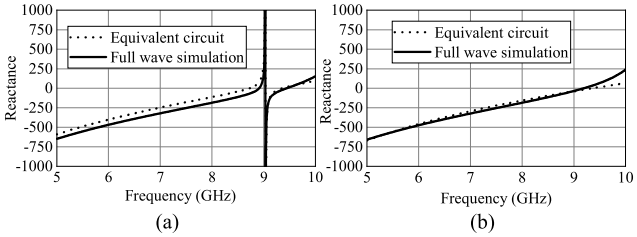

FIGURE 15. (a) The surface impedance of the single layer double-sided metallic strips for TE mode 60° incidence. (b) The surface impedance of the single layer double-sided metallic strips with shorting pins for TE mode 60° incidence.

of the dielectric, is added between two LC series circuits to equivalent the effect of the distance between two metallic strips. The impedance of the transmission line for TE mode incidence is given by,

$$Z_{TE} = \zeta_0 / \cos\theta \tag{5}$$

where $\zeta_0 = 377\ \Omega$ is the characteristics impedance of free space, θ is the incident angle of the electromagnetic wave. To verify the equivalent circuit, the double-sided metallic strip, whose length and width are fixed at 12.5 mm and 1 mm, is calculated by full wave simulation and equivalent circuit, respectively. In equivalent circuit model, the values of inductor and capacitor are 17.2 nH and 0.013 pF, respectively. The surface impedance calculated by equivalent circuit model is agree well with that calculated by full wave simulation, as shown in Fig. 15(a). Meanwhile, a resonance point is found at 9 GHz, indicating that the surface impedance of the double-sided metallic strip has a great change at resonance frequency. Note that because only a single layer metallic strip is analyzed, the calculated resonance frequency is higher than that shown in Fig. 8.

To solve this issue, double-sided metallic strips with shorting pins, which is shown in Fig. 14(b), is proposed to replace the double-sided metallic strips. The equivalent circuit model shows that the shorting pins between two metallic strips can eliminate the equivalent transmission line between two LC series circuits. Fig. 15(b) shows that the double-sided metallic strips with shorting pins can avoid abnormal resonance for TE mode incidence in xoz plane.

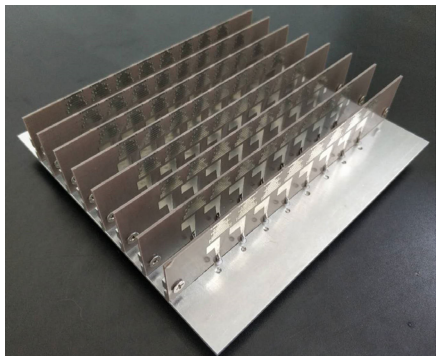

FIGURE 16. The fabricated 8 × 8 prototype.

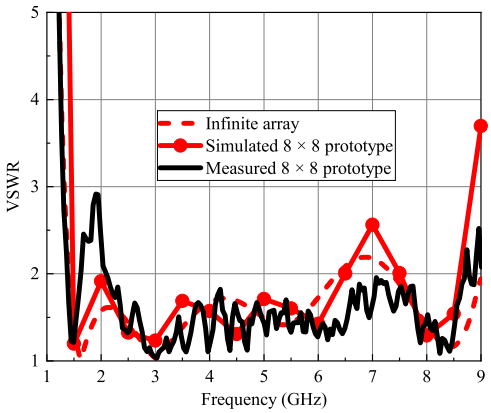

FIGURE 17. The simulated and measured active VSWR of the center element for broadside radiation.

IV. THE PERFORMANCE OF 8 × 8 PROTOTYPE

To verify the feasibility of the proposed array, an 8 × 8 prototype with a 160-mm × 160-mm aluminum ground plane, as shown in Fig. 16, is simulated, fabricated, and measured. The simulated and measured performance of the array is shown as follows.

A. RESULTS OF THE ACTIVE VSWR

The simulated active VSWR of the center element is carried out by Ansys HFSS. The measured active reflection coefficient of the center element is synthesized by the measured reflection coefficient of the center element and the mutual couplings between the center element and other elements, and the equation is given by,

$$\Gamma_{pq}(\theta_0, \varphi_0) = \sum_{m=1}^{M}\sum_{n=1}^{N} S_{mn,pq} e^{-j([m-p]d_x u + [n-q]d_y v)} \tag{6}$$

where $u = k\sin\theta_0\cos\varphi_0$, $v = k\sin\theta_0\sin\varphi_0$, $M = N = 8$ represents the number of elements along x- and y-directions, $d_x = d_y = 15$ mm represents the element's lattice spacings in the x- and y-directions, $S_{mn,pq}$ is the mutual coupling between elements mn and pq, and (θ_0, φ_0) represents the scanning angle of the array.

Fig. 17 shows the simulated and measured active VSWR of the center element for broadside radiation. The measured active VSWR agrees well with the simulated result over most

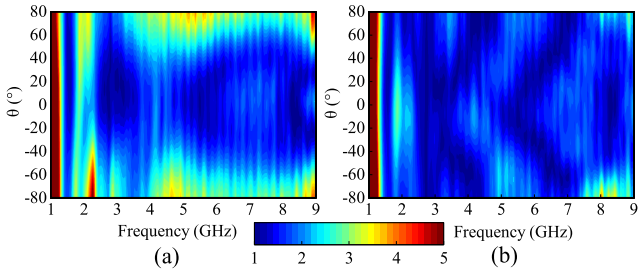

FIGURE 18. (a) Measured active VSWR of the center element for E-plane scanning with tapered excitation. (b) Measured active VSWR of the center element for H-plane scanning with tapered excitation.

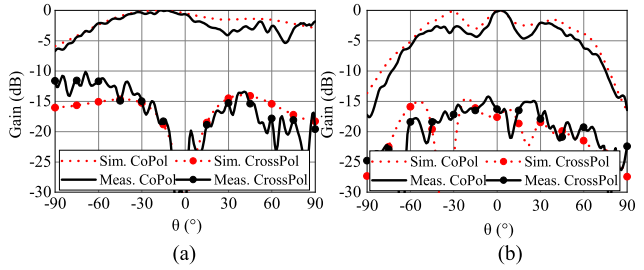

FIGURE 19. The simulated and measured center embedded element pattern in E-plane. (a) 2 GHz. (b) 8 GHz.

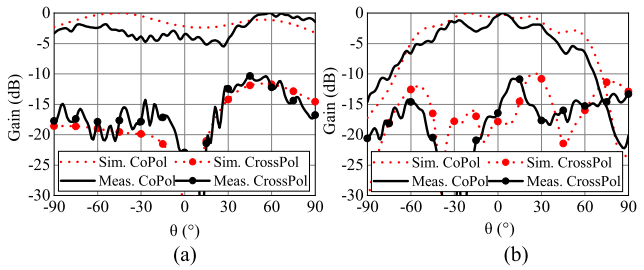

FIGURE 20. The simulated and measured center embedded element pattern in H-plane. (a) 2 GHz. (b) 8 GHz.

of operating band. The difference between the simulated and measured results is caused by the manufacturing and testing errors. Nonetheless, the measured active VSWR is smaller than 3 from 1.4 to 8.7 GHz. It is well-known that the edge effect of the finite array will cause the matching performance of the array becomes worse. One effective method to reduce the influence of the edge effect is using amplitude tapered to excite the array [20]. Fig. 18 shows the measured active VSWR of the center element for E- and H-planes scanning with tapered excitation. The active VSWR is smaller than 3.5 for scanning from $-40°$ to $60°$ and smaller than 4.5 for scanning from $-60°$ to -40° in E-plane in operating frequency. Besides, the active VSWR is smaller than 3 in operating frequency for scanning from $-60°$ to $+60°$ in H-plane. Note that the active VSWR of the finite array will be close to the results of the infinite array when the array size is large enough [21].

B. THE EMBEDDED ELEMENT PATTERN

Generally, the embedded element pattern is used to predict the scanning performance of a large array. It can be obtained

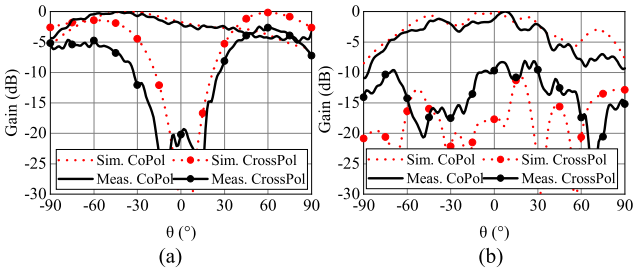

FIGURE 21. The simulated and measured center embedded element pattern in D-plane. (a) 2 GHz. (b) 8 GHz.

when the center element is excited and other elements terminated in matched loads. The simulated and measured embedded element pattern of the center element in E-, H- and D-planes are shown in Fig. 19, 20, and 21, respectively. Due to the testing error, some differences can be found between simulated and measured results. Nevertheless, the measured results show a similar tendency with the simulated results. Besides, we found that the cross-polarization of the center embedded element pattern in D-plane is worse than expected at low frequency. This issue can be improved when expanding the array size. Meanwhile, the embedded element pattern in all planes of a large array will approach the ideal element gain pattern, $G(\theta) = (4\pi A/\lambda^2)\cos\theta\,(1\text{-}|\Gamma(\theta)|^2)$, where A is the unit cell area, λ is the operating frequency, and $\Gamma(\theta)$ is the active reflection coefficient for scan angle θ [18].

C. THE SCANNING PATTERN OF THE PROTOTYPE ARRAY

The scanning pattern of the prototype array is measured by the unit excitation active element pattern (UEAEP) method [22]. In the measurement, the embedded element patterns of center 6×6 sub-array elements are measured when a single element is excited with other elements terminated in matched loads. Then, the scanning pattern of the center 6×6 sub-array is obtained by post processing.

Fig. 22 shows the simulated and measured realized gain of the center 6×6 sub-array at the broadside radiation. The measured result agrees well with the simulated results. Also, both simulated and measured results agree well with the idea aperture gain, indicating that the prototype array has a high efficiency. Besides, the simulated and measured cross-polarization at broadside radiation is also shown in the Fig. 22. The normalized cross-polarization of the array is lower than -15 dB for broadside radiation in operating band.

Fig. 23, 24, and 25 show the simulated and measured scanning pattern at 2 and 8 GHz. During post processing, the embedded element patterns are given the idea phase shifts which make the array scans at 0°, 30°, and 60° in E-, H-, and D-planes, respectively. As the frequency increases, the beam width of the scanning pattern become narrower. Due to the small array size, the beams did not direct to the expected direction when the array scans at large angle. This issue can be alleviated when expanding the array size. Meanwhile, the normalized cross-polarization for scanning to 60° in H- and D-planes is given in Fig. 24 and 25, respectively.

TABLE 1. Comparison of state-of-the-art arrays.

	BW	*Thickness**	θ_{max}	*Element Size**	*Layers*	*Feeding structure*
[8]	7.3:1	$0.1\lambda_{low}$	E-/H-45°	$0.46\lambda_{high} \times 0.46\lambda_{high}$	3	Complex
[9]	6.1:1	$0.12\lambda_{low}$	E-75°/H-60°	$0.41\lambda_{high} \times 0.41\lambda_{high}$	2	Complex
[10]	5.5:1	$0.14\lambda_{low}$	E-70°/H-55°	$0.35\lambda_{high} \times 0.35\lambda_{high}$	2	Middle
[12]	7.2:1	$0.067\lambda_{low}$	E-70°/H-45°	$0.48\lambda_{high} \times 0.48\lambda_{high}$	3	Complex
[23]	9:1	$0.1\lambda_{low}$	E-60°/H-30°	$0.48\lambda_{high} \times 0.48\lambda_{high}$	2	Complex
This work	**6.2:1**	$\mathbf{0.13\lambda_{low}}$	**E-/H-60°**	$\mathbf{0.44\lambda_{high} \times 0.44\lambda_{high}}$	**1**	**Simple**

* λ_{high} and λ_{low} are the highest and lowest operating frequency of the array, respectively.

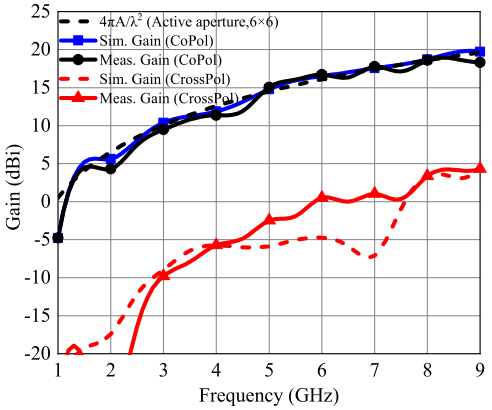

FIGURE 22. Simulated and measured realized gain of the prototype array for broadside radiation.

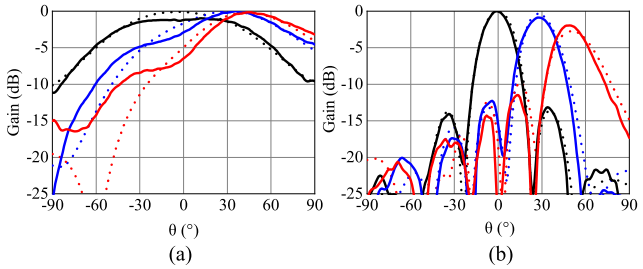

FIGURE 23. The simulated (dashed line) and measured (solid line) patterns for 0°, 30°, and 60° scans in E-plane.(a) 2 GHz. (b) 8 GHz.

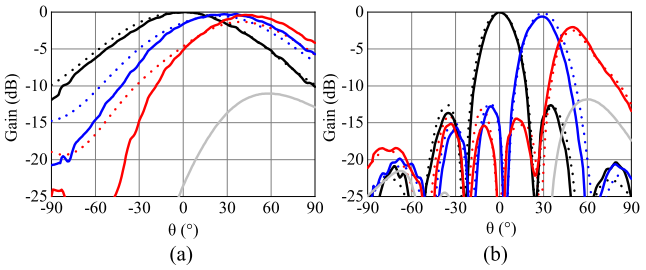

FIGURE 24. The simulated (dashed line) and measured (solid line) patterns for 0°, 30°, and 60° scans in H-plane. Grey line is the measured normalized cross-polarization ratio for 60° scanning. (a) 2 GHz. (b) 8 GHz.

It can be observed that the cross-polarization is lower than -10 dB and -6 dB for H- and D-planes scanning, respectively. Besides, the normalized cross-polarization for scanning to 60° in E-plane, which is not shown in Fig. 19, is lower than −25 dB at 2 and 8 GHz.

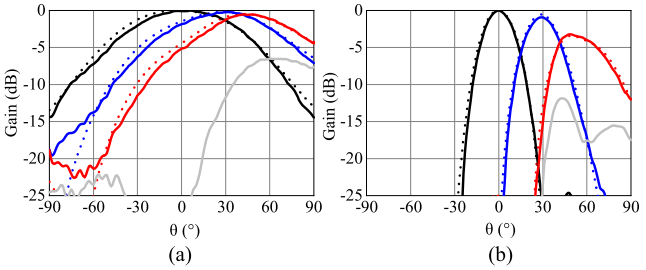

FIGURE 25. The simulated (dashed line) and measured (solid line) patterns for 0°, 30°, and 60° scans in D-plane. Grey line is the measured normalized cross-polarization ratio for 60° scanning. (a) 2 GHz. (b) 8 GHz.

Table 1 shows the comparison between this work and other wide-band tightly coupled dipole arrays. Unlike other designs, the proposed array can avoid external impedance transform structure or power divider located below the ground plane. Meanwhile, all components can be printed on a single layer dielectric, resulting in a light-weight and low-cost array. Most of all, the improvement did not sacrifice the electrically performance of the array.

V. CONCLUSION

In this article, a tightly coupled dipole array loaded with multilayer metallic strips is proposed. An equivalent circuit model is proposed to help design the loaded metal strip. Thanks to the loaded metal strips, the dipole has a low and smooth input impedance, making it can match with the coaxial easily and avoiding a matching circuit located below the ground plane. The proposed array can achieve a 6.2:1 bandwidth with ±60° scanning in all planes. Meanwhile, compared with the previous dipole with dielectric loading, the proposed tightly couple dipole can print on a single dielectric substrate, resulting in a light-weight and low-cost array. Finally, an 8 × 8 prototype array is simulated, fabricated and tested. The measured results show good agreement with the simulation, verifying the feasibility of the proposed array. Although the performance of the 8 × 8 prototype array is worse than the infinite array, a larger array size can be used in the future to improve the performance of the finite array.

REFERENCES

[1] J.-B. Yan, S. Gogineni, B. Camps-Raga, and J. Brozena, "A dual-polarized 2–18-GHz vivaldi array for airborne radar measurements of snow," *IEEE Trans. Antennas Propag.*, vol. 64, no. 2, pp. 781–785, Feb. 2016.

[2] G. C. Tavik, C. L. Hilterbrick, J. B. Evins, J. J. Alter, J. G. Crnkovich, J. W. de Graaf, W. Habicht, G. P. Hrin, S. A. Lessin, D. C. Wu, and S. M. Hagewood, "The advanced multifunction RF concept," *IEEE Trans. Microw. Theory Techn.*, vol. 53, no. 3, pp. 1009–1020, Mar. 2005.

[3] P. A. Dufilie, "Practical design of an octave-band stacked patch antenna phased array," in *Proc. IEEE Int. Symp. Phased Array Syst. Technol. (PAST)*, Oct. 2019, pp. 1–5.

[4] J. T. Logan, R. W. Kindt, and M. N. Vouvakis, "Low cross-polarization vivaldi arrays," *IEEE Trans. Antennas Propag.*, vol. 66, no. 4, pp. 1827–1837, Apr. 2018.

[5] J. T. Logan, R. W. Kindt, and M. N. Vouvakis, "A 1.2–12 GHz sliced notch antenna array," *IEEE Trans. Antennas Propag.*, vol. 66, no. 4, pp. 1818–1826, Apr. 2018.

[6] H. Wheeler, "Simple relations derived fom a phased-array antenna made of an infinite current sheet," *IEEE Trans. Antennas Propag.*, vol. 13, no. 4, pp. 506–514, Jul. 1965.

[7] B. Munk, R. Taylor, T. Durharn, W. Croswell, B. Pigon, R. Boozer, S. Brown, M. Jones, J. Pryor, S. Ortiz, and J. Rawnick, "A low-profile broadband phased array antenna," in *Proc. IEEE Antennas Propag. Soc. Int. Symp.*, vol. 2, Jun. 2003, pp. 448–451.

[8] J. P. Doane, K. Sertel, and J. L. Volakis, "A wideband, wide scanning tightly coupled dipole array with integrated balun (TCDA-IB)," *IEEE Trans. Antennas Propag.*, vol. 61, no. 9, pp. 4538–4548, Sep. 2013.

[9] E. Yetisir, N. Ghalichechian, and J. L. Volakis, "Ultrawideband array with 70° scanning using FSS superstrate," *IEEE Trans. Antennas Propag.*, vol. 64, no. 10, pp. 4256–4265, Oct. 2016.

[10] A. O. Bah, P.-Y. Qin, R. W. Ziolkowski, Y. J. Guo, and T. S. Bird, "A wide-band low-profile tightly coupled antenna array with a very high figure of merit," *IEEE Trans. Antennas Propag.*, vol. 67, no. 4, pp. 2332–2343, Apr. 2019.

[11] Y. Zhang and A. K. Brown, "Octagonal ring antenna for a compact dual-polarized aperture array," *IEEE Trans. Antennas Propag.*, vol. 59, no. 10, pp. 3927–3932, Oct. 2011.

[12] H. Zhang, S. Yang, S. Xiao, Y. Chen, and S. Qu, "Low-profile, lightweight, ultra-wideband tightly coupled dipole arrays loaded with split rings," *IEEE Trans. Antennas Propag.*, vol. 67, no. 6, pp. 4257–4262, Jun. 2019.

[13] S. S. Holland and M. N. Vouvakis, "The planar ultrawideband modular antenna (PUMA) array," *IEEE Trans. Antennas Propag.*, vol. 60, no. 1, pp. 130–140, Jan. 2012.

[14] J. T. Logan, R. W. Kindt, M. Y. Lee, and M. N. Vouvakis, "A new class of planar ultrawideband modular antenna arrays with improved bandwidth," *IEEE Trans. Antennas Propag.*, vol. 66, no. 2, pp. 692–701, Feb. 2018.

[15] B. A. Munk, "Broadband wire arrays," in *Finite Antenna Arrays and FSS*, 1st ed. Hoboken, NJ, USA: Wiley, 2003, ch. 6, pp. 181–213.

[16] N. Marcuvitz, *Waveguide Handbook*. New York, NY, USA: McGraw-Hill, 1951, vol. 10.

[17] S. S. Holland and M. N. Vouvakis, "The banyan tree antenna array," *IEEE Trans. Antennas Propag.*, vol. 59, no. 11, pp. 4060–4070, Nov. 2011.

[18] P. Hannan, "The element-gain paradox for a phased-array antenna," *IEEE Trans. Antennas Propag.*, vol. AP-12, no. 4, pp. 423–433, Jul. 1964.

[19] A. Ludwig, "The definition of cross polarization," *IEEE Trans. Antennas Propag.*, vol. AP-21, no. 1, pp. 116–119, Jan. 1973.

[20] D. Cavallo, W. H. Syed, and A. Neto, "Connected-slot array with artificial dielectrics: A 6 to 15 GHz dual-pol wide-scan prototype," *IEEE Trans. Antennas Propag.*, vol. 66, no. 6, pp. 3201–3206, Jun. 2018.

[21] H. Holter and H. Steyskal, "On the size requirement for finite phased-array models," *IEEE Trans. Antennas Propag.*, vol. 50, no. 6, pp. 836–840, Jun. 2002.

[22] D. M. Pozar, "The active element pattern," *IEEE Trans. Antennas Propag.*, vol. 42, no. 8, pp. 1176–1178, Aug. 1994.

[23] J. Zhong, A. Johnson, E. A. Alwan, and J. L. Volakis, "Dual-linear polarized phased array with 9:1 bandwidth and 60° scanning off broadside," *IEEE Trans. Antennas Propag.*, vol. 67, no. 3, pp. 1996–2001, Mar. 2019.

ZHIGUO JIANG (Student Member, IEEE) received the B.Sc. degree in electronic information science and technology from the University of Electronic Science and Technology of China (UESTC), Chengdu, China, in 2015, where he is currently pursuing the Ph.D. degree in radio physics.

His current research interests include reconfigurable antenna, wideband, and wide-scan array.

SHAOQIU XIAO (Member, IEEE) received the Ph.D. degree in electromagnetic field and microwave technology from the University of Electronic Science and Technology of China (UESTC), Chengdu, China, in 2003.

From January 2004 to June 2004, he joined UESTC as an Assistant Professor. From July 2004 to March 2006, he was a Research Fellow with the Wireless Communications Laboratory, National Institute of Information and Communications Technology (NICT), Singapore, with a focus on the planar antenna and smart antenna design and optimization. From July 2006 to June 2010, he was an Associate Professor with UESTC, where he was a Professor from August 2010 to December 2019. He visited the Ecole Normale Superieure de Cachan, Paris, France, as a Senior Research Scholar, from July 2015 to August 2015. Since January 2020, he has been a Professor with Sun Yat-sen University. He has authored/coauthored more than 300 technical journals, conference papers, books, and book chapters. His current research interests include planar antenna and phased array, computational electromagnetics, microwave passive circuits, and time reversal electromagnetics.

BING-ZHONG WANG (Senior Member, IEEE) received the Ph.D. degree in electronic engineering from the University of Electronic Science and Technology of China (UESTC), Chengdu, in 1988.

He joined UESTC, in 1984, where he is currently a Professor. He has been a Visiting Scholar with the University of Wisconsin–Milwaukee, WI, USA, as a Research Fellow with the City University of Hong Kong, Hong Kong, and a Visiting Professor with the Electromagnetic Communication Laboratory, Pennsylvania State University, University Park, PA, USA. His current research interests include computational electromagnetics, antenna theory and techniques, and time-reversed electromagnetics.